Transverse spin diffusion and spin rotation in very dilute, spin-polarized ^{3}He-^{4}He mixtures

D. Candela, D. R. McAllaster, and L-J. Wei
Laboratory for Low Temperature Physics, Physics and Astronomy Department, University of Massachusetts at Amherst, Amherst, Massachusetts 01003
(Received 3 June 1991)

We report measurements of the transverse-spin-diffusion coefficient $D_\perp$ and the spin-rotation parameter $\Omega\tau_\perp$ for two very dilute ^{3}He-^{4}He mixtures ($x_3=1.82\times10^{-3}$ and 6.26×10^{-4}) spin polarized by an 8-T magnetic field. Brute-force spin polarization up to 40% was achieved at the lowest temperature, 6 mK. We find that $\Omega\tau_\perp$ increases monotonically as the temperature is reduced through the Fermi temperature T_F, in disagreement with the only previous experiment but in good agreement with recent theory. Unlike the earlier experiment, which measured spin echoes, the present experiments employed a spin-wave technique that avoids nonlinear excitation of the spin field. We compare our results with the recent calculations of Jeon and Mullin for spin transport in dilute gases with arbitrary polarization and degeneracy. The best fit to the data is obtained by scaling the quasiparticle interaction $V(q)$ proposed by Ebner by a modest factor, 1.07. The corresponding s-wave scattering length is $a=-1.21$ Å. Good agreement is found for $\Omega\tau_\perp(T)$ at both concentrations and all temperatures, and for $D_\perp/\Omega\tau_\perp(T)$ apart from the lower concentration at $T<20$ mK. The discrepancy in $D_\perp/\Omega\tau_\perp$ at the lowest temperatures and x_3 could be explained by an unanticipated polarization dependence or by modification of the spin-wave boundary condition by processes occurring at the interface between the mixture and the silica cavity wall.

I. INTRODUCTION

The transport coefficients of spin-polarized quantum fluids have been the subject of recent theoretical and experimental investigation[1,2] because they directly probe quasiparticle scattering. Strongly interacting systems such as ^{3}He liquid are, at present, theoretically intractable, so much interest has focused on dilute systems (quantum gases).[3–7] Although the static properties are trivially given by ideal-gas theory, the transport coefficients exhibit subtle quantum effects such as cross coupling of spin, heat, and particle currents and the propagation of spin waves.[2–4] Some of these effects have been observed in polarized gases[8,9] far above their quantum degeneracy temperatures $T\gg T_{F,B}$. Quantum spin-transport effects have also been observed in highly degenerate ($T\ll T_F$) metals and Fermi liquids,[10–15] for which the elementary excitations effectively form a dilute Fermi gas. None of these systems allow the properties of a quantum gas to be probed in the crossover region $T\sim T_F$, nor can they be significantly spin polarized by available laboratory fields. Experiments at high polarization and $T\sim T_F$ have become particularly desirable with the recent appearance of transport calculations[6,7] covering these conditions.

In practice, the only neutral quantum gas that may be cooled through T_F without condensing is a dilute solution of ^{3}He in superfluid^4 He.[16] For temperatures $T<1$ K, phonon and roton excitations of the ^{4}He solvent are negligible, and the dissolved ^{3}He atoms form a gas with renormalized mass $m=2.255m_3$ (where m_3 is the bare atomic mass),[17] and greatly reduced interparticle interaction. The degeneracy temperature T_F may be freely varied by choosing the ^{3}He atomic concentration x_3. An applied magnetic field B_0 strongly spin polarizes the system if both k_BT and k_BT_F are less than the spin-flip energy $\hbar\gamma B_0$, where γ is the ^{3}He gyromagnetic ratio. In this paper we report measurements of transverse spin transport in very dilute ^{3}He-^{4}He mixtures with brute-force polarizations up to 40%, and temperatures from $0.2T_F$ to $2.4T_F$. The only previous experiment[18] reported results that are in strong disagreement with theory. Our experiments, using a different technique, have resolved this discrepancy.[19]

Spin transport in a polarized system is inherently richer and more complicated than in an unpolarized system. Spin polarization establishes a preferred direction in spin space (along $\mathbf{B}_0$ in equilibrium), and quantum exchange establishes a preferred rotation direction about the polarization, which is opposite for fermions and bosons.[2–6] Letting M_z be the spin density along the polarization, and $M_+\equiv M_x+iM_y$, the corresponding spin currents $\mathbf{J}_z, J_+$ for small deviations from equilibrium may be written[2]

$$\mathbf{J}_z=-D_\parallel\nabla M_z,\quad \mathbf{J}_+=-\frac{D_\perp}{1+i\Omega\tau_\perp}\nabla M_+\ . \tag{1}$$

The spin-diffusion coefficient for an unpolarized system D, is replaced upon polarization by the three quantities $D_\parallel$, $D_\perp$, and $\Omega\tau_\perp$. The longitudinal and transverse-spin-diffusion coefficients are proportional to distinct microscopic relaxation times,[6,20] $D_\parallel\propto\tau_\parallel$ and $D_\perp\propto\tau_\perp$. For low temperatures $T\ll T_F$, the longitudinal relaxation time $\tau_\parallel$ grows as T^{-2} due to the usual phase-space considerations for a degenerate Fermi system. The transverse relaxation time $\tau_\perp$ is predicted to have an unusual behavior: at any nonzero polarization, $\tau_\perp$ tends to a constant as T ap-

proaches zero.[6] The reason is that the phase space for spin-flip scattering, which governs transverse relaxation, includes the shell between spin-up and spin-down Fermi spheres. No experiment to date (including the one reported here) has reached sufficiently low temperature and high polarization to observe the difference between $D_{\parallel}$ and $D_{\perp}$.

Conversely, a nonzero $\Omega\tau_{\perp}$, which is termed spin rotation, has profound effects upon spin transport that have been observed in a number of experiments[8-15] (common notations are $\Omega\tau_{\perp}=\Omega_{\rm int}\tau_{\perp}=\mu M=-\lambda\omega_0\tau_D$). The internal frequency Ω appears in the theory as a precession frequency of the spin current about the polarization, and spin rotation dominates transverse transport when this frequency is greater than the relaxation rate τ_1^{-1}. In a degenerate system, Ω is considered a consequence of the Landau molecular field and is given by the Fermi-liquid parameters F_0^a and F_1^a, as discussed by Leggett.[21] He derived an equation for the spin current (with $D_{\parallel}=D_{\perp}$) for arbitrarily large deviations of **M** from equilibrium, and predicted a nonexponential decay and phase shift of the spin echo produced by a ϕ-180° NMR experiment. This Leggett-Rice effect was observed by Corruccini *et al.* in ^{3}He and relatively concentrated ^{3}He-^{4}He mixtures.[11] Equation (1) above with $D_{\parallel}=D_{\perp}$ is the small-deviation limit of the Leggett equation, and it predicts[12] spin-wave propagation when $\Omega\tau_{\perp}>1$. (Spin waves in the extreme collisionless limit $\Omega\tau_{\perp}\gg1$ were discussed much earlier by Silin.[22]) The predicted spin waves were observed in several degenerate Fermi systems.[10,12,13,15]

Bashkin[3] and Lhullier and Laloë[4] showed that a polarized gas far above its degeneracy temperature also obeys the Leggett equation. Even though the velocity distribution is classical, quantum exchange dominates collisions when the de Broglie wavelength exceeds the atomic size, resulting in $\Omega\tau_{\perp}\neq0$. This "identical-spin rotation effect" has been observed via spin waves in polarized ^{3}He and atomic hydrogen gases.[8,9] A plot of the polarization-temperature plane (Fig. 1) suggests that the Leggett-Rice and identical-spin rotation effects are closely related.[23] As Fig. 1 shows, a very dilute ^{3}He-^{4}He mixture in a strong magnetic field is well suited for exploring the crossover between these two effects. Gully and Mullin reported a spin-echo experiment under these conditions,[18] which showed an unexpected decline in $\Omega\tau_{\perp}$ (after reaching a maximum value of 1.6) as the temperature was lowered to T_F.

Recent kinetic-theory calculations have filled the gaps in the polarization-temperature plane.[6] It was shown that $\Omega\tau_{\perp}$ and $D_{\perp}$ interpolate smoothly between the nondegenerate and degenerate regimes, and that anisotropic relaxation with $\tau_{\perp}<\tau_{\parallel}$ only occurs at much lower temperatures than were reached in the experiment of Ref. 18. The present work was motivated by these quantitative predictions for the half-polarized, half-degenerate regime that clearly disagreed with the only existing data. We have measured transverse spin transport in the same regime as Ref. 18, using a different technique (linear spin waves). Unlike Ref. 18, we find that $\Omega\tau_{\perp}$ rises monotonically with lowering temperature. Thus, the discrepancy between theory and experiment is resolved in favor of the former. Possible explanations for the anomalous results of the earlier experiment are discussed in Sec. IV below.

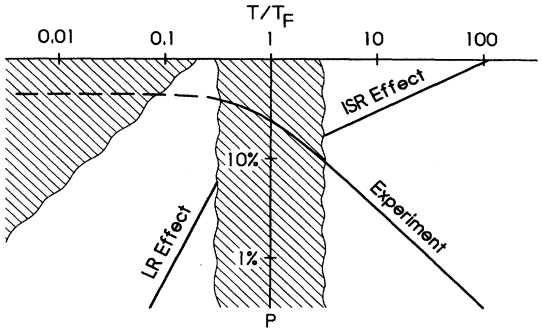

FIG. 1. Schematic plot of the polarization vs temperature plane for a weakly interacting Fermi gas. In the degenerate regime $T\ll T_F$, the Leggett-Rice effect occurs above the line marked "LR effect." In the Boltzmann regime $T\gg T_F$, the identical-spin rotation effect occurs above the line marked "ISR effect." The shaded strip in the center shows the crossover region $T\sim T_F$, while the shaded wedge to the left shows the region where anisotropic spin relaxation ($\tau_{\perp}\ll\tau_{\parallel}$) occurs. Quantitative predictions were unavailable for either shaded region prior to the generalized calculations of Jeon and Mullin (Ref. 6). The curve marked "Experiment" shows the polarization vs temperature for a very dilute ^{3}He-^{4}He solution in a strong magnetic field, which is suitable for probing the crossover between the ISR and LR effects. This system should also display anisotropic spin relaxation when cooled to lower temperatures than have been achieved to date (dashed section of curve). This figure has been drawn for conditions appropriate to one of our experimental runs ($x_3=6.26\times10^{-4}$, $B_0=7.956$ T).

The plan of this paper is as follows: Section II reviews the spin-wave technique for measuring spin transport, and develops it for the geometry we have used for these experiments. Section III describes the apparatus and experimental procedures. Section IV presents the results of our measurements for $D_{\perp}/\Omega\tau_{\perp}$ and $\Omega\tau_{\perp}$ for two very dilute solutions polarized by an 8-T field, and discusses their relation to the recent theoretical advances.

II. SPIN-WAVE TECHNIQUE

In a typical NMR experiment, the sample is subject to a static field $\mathbf{B}_0(\mathbf{r})$ that varies slightly with position $\mathbf{r}$, and a transverse $\mathbf{B}_1$ coil is used to measure the frequency-dependent transverse susceptibility averaged over the sample, $\chi(\omega)$. As shown in Ref. 12, $\chi(\omega)$ may be expressed as an infinite sum of Lorentzian peaks,

$$\chi(\omega)\propto\sum_{\alpha}\frac{C^{\alpha}}{\omega^{\alpha}-\omega}\ , \tag{2}$$

where ω^{α} are the complex eigenvalues of the following equation:

$$\frac{D_{\perp}}{i-\Omega\tau_{\perp}}\nabla^2M_+^{\alpha}+\gamma B_0(\mathbf{r})M_+^{\alpha}=\omega^{\alpha}M_+^{\alpha}\ . \tag{3}$$

The eigenfunction $M_+^{\alpha}(\mathbf{r})$ represents the transverse mag-

netization when mode α is excited and must satisfy an appropriate boundary condition at the cell wall. The first term describes transverse diffusion according to Eq. (1), while the second term accounts for precession about the static field. In a pulsed NMR experiment such as reported here, the complex Fourier transform of the free-induction decay gives $\chi(\omega)$, provided the tipping angle is small enough for the system response to be linear.

For the simplified conditions of an infinite sample in a perfectly uniform B_0 field, Eq. (3) has plane-wave solutions $M_+(\mathbf{r})=\exp(i\mathbf{k}\cdot\mathbf{r})$ with dispersion relation

$$\omega=\gamma B_0+\frac{D_\perp}{\Omega\tau_\perp-i}k^2 . \tag{4}$$

The mode weights C^α in Eq. (2) are computed from the inner product of the B_1 field distribution with the corresponding modes. With uniform B_0 and B_1, the only nonzero weight is for the $k=0$ wave, which carries no information about $D_\perp$ or $\Omega\tau_\perp$. Typically, spin-wave experiments have employed a static field with a gradient $B_0(\mathbf{r})=B_0(\mathbf{r}_0)+\mathbf{G}\cdot(\mathbf{r}-\mathbf{r}_0)$ in order to couple to nonzero wave vectors.[9,12,15] In the collisionless limit $\Omega\tau_\perp\gg1$, Eq. (3) has the form of the Schrödinger equation for a particle with potential energy $\gamma B_0(\mathbf{r})$. The gradient $\mathbf{G}$ acts as a force confining the modes to the low-field part of the sample cell (when $\Omega\tau_\perp>0$ as it is for very dilute ^{3}He-^{4}He), and the boundary condition for the spin field at the cell wall is important in determining the NMR response.[5,12]

For a one-dimensional system, the eigenfunctions in a uniform gradient are Airy functions (as are the eigenstates of a quantum particle subject to a uniform force). Past spin-wave experiments have used rectangular or cylindrical boxes to confine the sample, with the gradient along a symmetry direction to approximate the one-dimensional case. For several reasons we have found it advantageous to use a different geometry for the cell that confines the sample and determines the spin-wave modes. One difficulty with a box-shaped cell is the near degeneracy of modes associated with different quantum numbers transverse to the main gradient axis, which results in a characteristic fine structure on each of the main Airy modes.[12] Unless eliminated by extremely accurate field shimming,[9(b)] this effect makes it difficult to measure $\Omega\tau_\perp$ (which determines the mode widths). Another problem with the box-shaped cell is accurate construction from a suitable material. From the expected range of $D_\perp/\Omega\tau_\perp$ and the minimum uniform gradient readily achievable in an 8-T field, we estimated a suitable cell dimension to be ~1 mm. At the same time it was desired to fabricate the cell with surfaces formed by free solidification of amorphous silica, as past experiments on pure ^{3}He had shown that this produced a reflecting boundary condition[12] (due perhaps to the atomic smoothness and relatively weak nuclear magnetism).

The cavity design addressing these problems is a sphere. It is straightforward to fabricate accurate 1-mm-diam spherical cavities in silica using glass-blowing techniques. A uniform gradient is used to confine the modes against one side of the sphere. The lowest few modes are then nondegenerate and well spaced in frequency because confinement in the gradient direction against a spherical wall also implies confinement in the directions transverse to the gradient. Finally, the system retains azimuthal symmetry about the gradient direction despite any small misalignment of the latter with respect to the cell axis. A channel for filling the cell and providing thermal contact may be placed in the direction opposite the gradient, as all of the spin-wave modes decay exponentially in this direction.

We now show how to apply the matrix solution method of Ref. 12 to the problem of a spherical cavity with a uniform gradient. In this method, the spin-wave modes are expanded in terms of the solutions to the gradient-free problem. For a sphere these are of the form

$$M_+(r,\theta,\phi)=j_l(x_{nl}r)Y_{lm}(\theta,\phi) ,$$

where j_l is a spherical Bessel function,[24] Y_{lm} in a spherical harmonic, and the constants x_{nl} depend upon the boundary condition. If the B_1 field is uniform it will only couple to the $m=0$ modes, to which we now specialize. For a zero spin-current boundary condition, we find the mode frequencies are $\omega^\alpha=\omega_0-\gamma GRf^\alpha$, where ω_0 is the local Larmor frequency at the center of the sphere, R is the sphere radius, and f^α are the eigenvalues of the matrix equation

$$\sum_{n'l'}H_{nln'l'}\psi^\alpha_{n'l'}=f^\alpha\psi^\alpha_{nl},\quad \sum_{nl}|\psi^\alpha_{nl}|^2=1 . \tag{5}$$

Here the matrix $\underline{H}$ is given by

$$H_{nln'l'}=\Omega_{nln'l'}-x_{nl}^2\Delta^3\delta_{nn'}\delta_{ll'} , \tag{6}$$

where x_{nl} is the $(n+1)$th zero of $dj_l(x)/dx$ and the gradient and spin-transport coefficients are combined in the dimensionless quantity $\Delta^3\equiv D_\perp/[\gamma GR^3(\Omega\tau_\perp-i)]$. The matrix $\underline{\Omega}$ contains the matrix elements of a linear gradient in dimensionless form,

$$\Omega_{nln'l'}=\frac{\lambda+1}{[(2\lambda+1)(2\lambda+3)]^{1/2}}\times\int_0^1 dx\, x^2c_{nl}c_{n'l'}j_l(xx_{nl})xj_{l'}(xx_{n'l'}) . \tag{7}$$

In this equation, λ is the smaller of l and l', the matrix element is zero unless $l'=l\pm1$, and

$$c_{nl}\equiv\left[\int_0^1 dx\, x^2j_l(xx_{nl})^2\right]^{-1/2}$$

is a normalization constant. Finally, for a uniform B_1 field, the mode weights are computed as $C^\alpha=\eta^\alpha_{00}\psi^\alpha_{00}$, where the matrix η is defined by $\sum_\alpha\eta^\alpha{}_{nl}\psi^\alpha_{n'l'}=\delta_{nn'}\delta_{ll'}$. The indices n and l run from zero to infinity, but for numerical calculations the sums are truncated at some $n_{\max}$ and $l_{\max}$. By examining how the computed frequencies vary as $n_{\max}$ and $l_{\max}$ are varied within a constraint of matrix dimension $(n_{\max}+1)(l_{\max}+1)\le N$, it was found to be much more important to include high-l values than high-n values for accurate determination of the mode frequencies. The results presented here were calculated with $n_{\max}=6$, $l_{\max}=31$ ($N=224$).

For any finite $\Omega\tau_\perp$, Δ is complex and the matrix $\underline{H}$ is non-Hermitian. In this case the eigenvectors ψ^α are not

mutually orthogonal and the mode frequencies ω^α have nonzero imaginary parts, giving finite widths to the spin-wave peaks according to Eq. (2). These equations may be solved as they stand for $\omega^\alpha(\Delta)$ and $C^\alpha(\Delta)$, but we have made a further approximation to simplify the data fitting. First, we have computed the dimensionless frequencies f^α for a range of *real* Δ, corresponding to $\Omega\tau_\perp=\infty$ (Fig. 2). For real Δ, $\underline{H}$ is Hermitian and the formula for the weights simplifies to $C^\alpha=|\psi^\alpha_{00}|^2$. Then, assuming each f^α is an analytic function of Δ, a finite-difference approximation to the Cauchy-Riemann equations gives

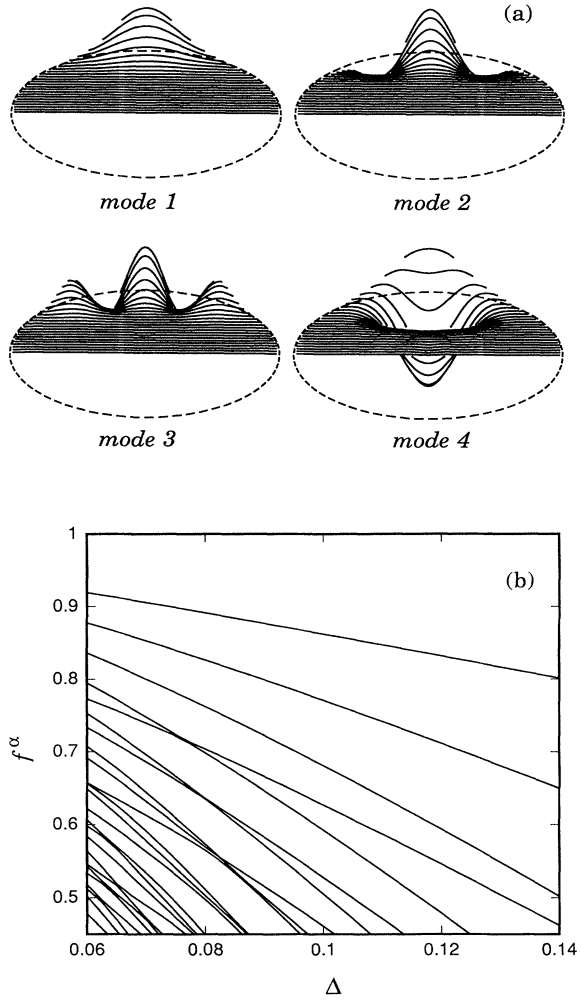

FIG. 2. Results of numerical calculation of the standing spin-wave modes in a sphere with a reflecting boundary condition and a uniform field gradient. (a) The four highest-frequency spin-wave modes for gradient parameter $\Delta=0.1$. The mode amplitude is plotted vertically as a function of position within the sphere in cylindrical coordinates. (b) Dimensionless frequencies f^α for the highest-frequency modes as a function of Δ. The top of the plot ($f^\alpha=1$) corresponds to the local Larmor frequency at the tip of the sphere, and there are infinitely many modes beyond those graphed in the negative f^α direction. Note the smaller slope of the fourth-highest mode frequency at $\Delta=0.1$, corresponding to its different spatial structure.

$$f^\alpha(\Delta)\approx f^\alpha(\mathrm{Re}\Delta)+i\,\mathrm{Im}\Delta\frac{\partial f^\alpha(\mathrm{Re}\Delta)}{\partial\,\mathrm{Re}\Delta}\ . \tag{8}$$

Generally this is only a good approximation for small $\mathrm{Im}\Delta$ or $\Omega\tau_\perp\gg1$, but we expect it is accurate for a wide range of $\Omega\tau_\perp$ because the f^α are nearly linear functions of Δ (Fig. 2). Equation (8) enables a rapid evaluation of the mode frequencies and widths as a function of $D_\perp/\Omega\tau_\perp$ (which primarily determines the frequencies) and $\Omega\tau_\perp$ (which primarily determines the widths), starting with a table of $f^\alpha(\mathrm{Re}\Delta)$ computed by diagonalizing Hermitian matrices.

Two assumptions implicit in this discussion must be checked if the above analysis is to be used for quantitative measurements. The first is the boundary condition on the transverse magnetization $\nabla M_+\cdot\mathbf{n}=0$, corresponding to zero spin current into the wall ($\mathbf{n}$ is the normal to the wall). This is appropriate if the wall is magnetically inert. Transverse (t_2-like) spin relaxation in a layer adjacent to the wall modifies the boundary condition to a mixed condition on M_+ and $\nabla M_+\cdot\mathbf{n}$. Following Ref. 12, we estimate that this effect would be negligible in our experimental conditions, even if there were a complete monolayer of ^{3}He near the wall with full Curie-law susceptibility.

The second assumption is a long-wavelength approximation made in the derivation of Eq. (1) from a kinetic equation.[21] In terms of plane waves, the condition is $k^{-1}\gg\min(v_F\tau_\perp, v_F/\Omega)$, where v_F is the Fermi velocity (or thermal velocity for $T\gg T_F$). Using Eq. (4) to estimate k from the frequency shift away from the Larmor frequency γB_0, we find that this condition is well satisfied by the present experiments, with, for example, $k^{-1}\approx170(v_F/\Omega)$ for the first spin-wave mode at the lowest temperatures.

III. EXPERIMENTS

The experiments were carried out in two different sample cells of similar construction. The spin-wave cavities were blown from fused silica tube stock with an initial size of 2.5 mm OD×0.2 mm ID. They were immersed in a bath that precisely matched the index of refraction of silica (2-fluorotoluene at 48 °C), which rendered the outer wall invisible and allowed accurate measurements of the inside wall with a toolmaker's microscope. The measurements were fit to a circular profile using points successively further from the tip. The cavities selected for use in the experiments had fit radii R which were nearly constant over the distance from the tip sampled by the spin waves (inferred from mode plots like Fig. 2). The cavities used for the first and second cells had $R=0.0386(13)$ and 0.0597(25) cm, respectively.

A small ^{195}Pt-NMR thermometer[25] was placed in the bottom section of the silica spin-wave cavity, which was glued into a silver cell body. The cell enclosed a heat exchanger made of pressed silver powder, as well as a small open volume for a vibrating wire viscometer (Fig. 3). The silver rod from which the cell body was machined extended up from the bore of an 8-T superconducting magnet to the mixing chamber of a dilution refrigerator, interrupted

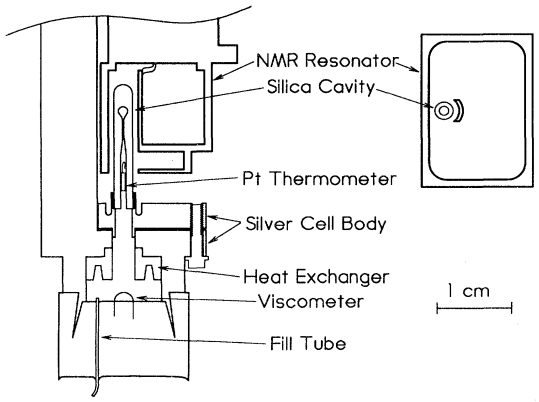

FIG. 3. Vertical cross section through the second sample cell. Inset at right shows a horizontal cross section through the inductive section of the ^{3}He NMR resonator at the level of the spherical cavity.

only by a squeeze connector that used differential thermal contraction to make a high conductivity joint. The fill line of the second cell incorporated a small reservoir in the high-field region, and the sample volume was chosen to have a free surface in this reservoir. All of the results we report are for zero sample pressure.

Electrical resonators for ^{3}He and ^{195}Pt NMR surrounded, but did not touch, the spin-wave cavity. The resonators were thermally anchored to the still (0.8 K) by their coaxial transmit-receive cables, and were mechanically anchored to the silver cell by an arrangement of graphite spacers. The heat leak through this support to the cell was rendered negligible by interrupting it with a copper plate thermally anchored to an intermediate stage of the refrigerator (at 100 mK). The ^{3}He resonator was designed using a numerical field-mapping technique to maximize the sample filling factor and B_1 field uniformity. The inductive section consists of a copper box with an off-center, curved vertical post (Fig. 3). When radio-frequency current flows down the post, across the floor of the box, and up its sides, an intense B_1 field is created between the post and the nearest box wall. The spin-wave cavity projects up into this space through a hole in the box floor.

The primary thermometer for these experiments was a ^{3}He melting-pressure thermometer (MPT) similar to that described by Greywall,[26] attached to the silver rod just below the mixing chamber. The melting pressure scale reported in Ref. 27 was used. The high-field ^{195}Pt-NMR thermometry we have developed[25] was used for the experiments with the first sample cell, but not with the second cell due to equipment failure. The platinum thermometer is calibrated against the MPT at high temperature (30–100 mK), and then serves, in effect, to verify good thermal contact between the sample and the MPT at the lowest temperatures, as well as checking for systematic error in the pressure calibration of the MPT.[25] The thermal arrangements for the two sample cells were the same, so we estimate that all temperatures reported here are accurate to a fraction of a mK.

The homodyne NMR spectrometer employed quadrature detection, and pulse gating and digitizer clocking synchronous with a master synthesizer operating at the Larmor frequency.[28] A PIN-diode duplexer as described by Hoult and Richards[29] was used to prevent saturation of the low-noise room-temperature preamplifier during transmitter pulses. The free-induction decay was recorded after a single pulse that tipped the magnetization by 6°. Usually 8192 complex time-domain points were acquired at several different digitizing frequencies, and ten of these signals were averaged together before Fourier transformation yielding $\chi(\omega)$.

NMR techniques were used to obtain the most accurate values for two parameters used in the data analysis, the ^{3}He atomic concentration x_3 and the gradient strength G. The amplitude of the free-induction decay immediately following a pulse was directly fit to the known temperature-dependent susceptibility of a weakly interacting Fermi gas.[30] Excellent fits were obtained (Fig. 4), giving $x_3=[1.82(3)]\times10^{-3}$ for the sample used in the first cell, and $x_3=[6.26(45)]\times10^{-4}$ for the sample used in the second cell. The corresponding Fermi temperatures are 39.8 and 19.5 mK. To establish the field gradient, the currents in all of the magnet shim coils (comprising spherical harmonics with $l=0,1,2$) were first adjusted to minimize the width of the NMR line, and then the current was changed in the shim coil designed to produce a vertical gradient. A least-squares fit of $\chi(\omega)$ measured via NMR to the shape of the sample cavity then yielded $G=-3.6(2)$ G/cm for the higher concentration data and $G=-2.0(1)$ G/cm for the lower concentration data. The negative sign here denotes a gradient making B_0 smallest at the closed (top) end of the cavity, as is necessary to trap spin waves when $\Omega\tau_\perp>0$.

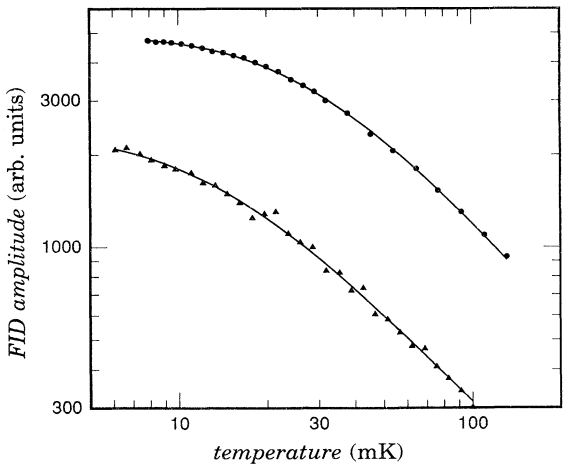

FIG. 4. Initial amplitude of the free-induction decay following a 6° tipping pulse, for the higher concentration (●) and lower concentration (▲) samples. The curves show least-squares fits of this data to the theoretical susceptibility of a weakly interacting Fermi gas, which were used to determine the concentrations as $x_3=[1.82(3)]\times10^{-3}$ and $x_3=[6.26(45)]\times10^{-4}$, respectively. The low-temperature deviation from Curie-law (T^{-1}) behavior is due mainly to degeneracy and occurs at a lower temperature for the sample with lower x_3.

IV. RESULTS AND DISCUSSION

With the magnet shimmed for a uniform gradient, the spin-wave resonances became evident at low temperatures as a series of peaks [Fig. 5(a)] at the low-frequency edge of the NMR line $\chi(\omega)$. This is consistent with the theory outlined above as well as a number of spin-wave experiments on other systems[9,12,15] (but not one early experiment[13] on ^{3}He-^{4}He). At each temperature, the measured $\chi(\omega)$ near the low-frequency line edge was fit to a sum of Lorentzian peaks with independent frequencies, widths, and heights. Excellent fits are obtained (Fig. 5) in agreement with Eq. (2). The mode frequencies and widths were then fit to the spin-wave theory using Eq. (8), thereby determining the complex parameter Δ. The mode weights C^α are not used in this fitting procedure, but we have checked that the measured weights are in good agreement with the theory [Fig. 5(b)].

Combining Δ from the fit to $\chi(\omega)$ with the measured gradient G and cavity radius R, one obtains the spin-transport quantities $D_\perp/\Omega\tau_\perp$ and $\Omega\tau_\perp$. These are plotted in Figs. 6 and 7 for the two concentrations x_3. We

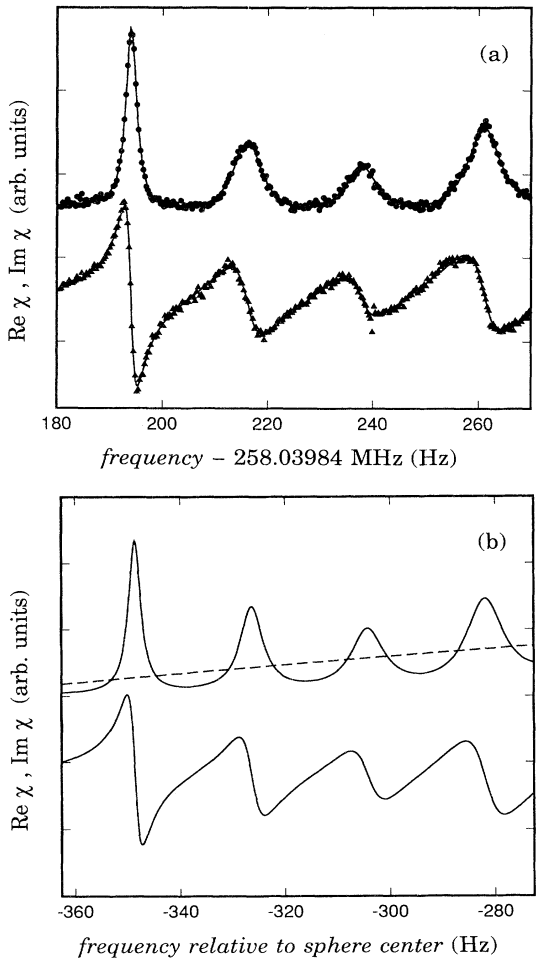

FIG. 5. (a) Measured complex susceptibility $\chi(\omega/2\pi)$ for a dilute solution with $x_3=6.26\times10^{-4}$ in a static field $B_0=7.956$ T, at temperature $T=6.085$ mK. Circles are the absorption Imχ and triangles are the dispersion Reχ. Only a small portion of the spectrum is shown, in the vicinity of the low-frequency edge of the line. The curves show a simultaneous fit of Reχ and Imχ to the sum of four complex Lorentzian peaks and a quadratic background. The peak frequencies and widths from this fit are used to determine the spin-transport quantities $D_\perp/\Omega\tau_\perp$ and $\Omega\tau_\perp$. (b) Complex susceptibility predicted by the spin-wave calculation for the fit values of $D_\perp/\Omega\tau_\perp$ and $\Omega\tau_\perp$ (solid curves). Note that the relative peak heights (which were not used in the determination of $D_\perp/\Omega\tau_\perp$ and $\Omega\tau_\perp$) are in good agreement with the data. The dashed curve shows the predicted absorption in the absence of spin transport, a section of a parabola.

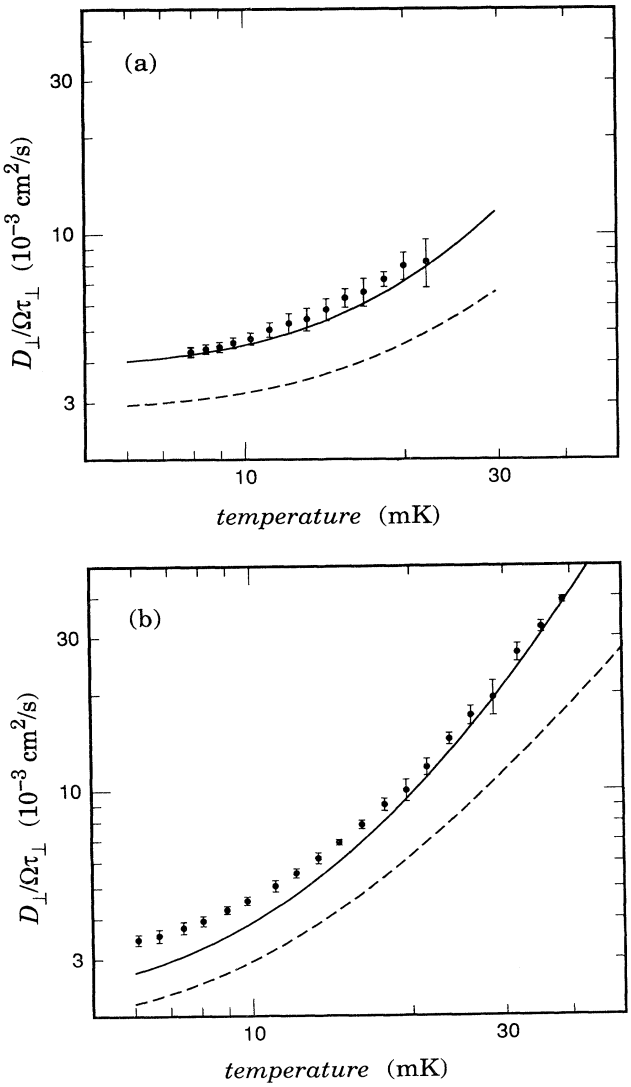

FIG. 6. Spin-wave dispersion $D_\perp/\Omega\tau_\perp$ for (a) $x_3=1.82\times10^{-3}$ and (b) $x_3=6.26\times10^{-4}$. The applied static field was $B_0=8.001$ T for the larger x_3 and $B_0=7.956$ T for the smaller x_3. The points with error show experimental results. The solid curves show calculations using the method of Refs. 6 and 7, for a quasiparticle interaction $V(q)$ that is 7% stronger than the Ebner $V(q)$. The dashed curves show an s-wave calculation, using the same $V(0)$.

present these two quantities rather than their product $D_\perp$ because the spin-wave mode frequencies are determined almost exclusively by $D_\perp/\Omega\tau_\perp$, and the mode widths (relative to their frequency separations) are determined almost exclusively by $\Omega\tau_\perp$. The two quantities plotted are therefore nearly independent measurements, subject to different sources of systematic error. For example, errors in G or R would mainly affect $D_\perp/\Omega\tau_\perp$ while an unanticipated surface relaxation process would mainly affect $\Omega\tau_\perp$.

It is clear from Fig. 7 that the maximum in $\Omega\tau_\perp(T)$ in the vicinity of T_F reported in Ref. 18 is not confirmed. Our $\Omega\tau_\perp$ data extend from $0.20T_F$ to $0.95T_F$ at $x_3=1.82\times10^{-3}$ and from $0.31T_F$ to $2.44T_F$ at $x_3=6.26\times10^{-4}$. For both concentrations they are consistent with a monotonic rise of $\Omega\tau_\perp$ with decreasing T, in agreement with theoretical expectations.[7] A possible reason for the anomalous results of Ref. 18 is the spin-echo technique, which involves large deviations of the magnetization from equilibrium. When generalized to $\tau_\parallel\neq\tau_\perp$, the Leggett equation contains only the same three quantities $D_\parallel$, $D_\perp$, and $\Omega\tau_\perp$ that describe linear transport, so this theory says that the same information is obtainable from linear experiments like the present work, and large-deviation experiments like spin-echo experiments. At least one other experiment[31] has found disagreement with the Leggett equation at large tipping angles, and there is also theoretical[32] work predicting corrections to this equation when the magnetization is rotated far from equilibrium. We note that no spin-echo experiment has observed $|\Omega\tau_\perp|\geq4$, while we have observed $|\Omega\tau_\perp|\approx10$ in the present work (Fig. 7).

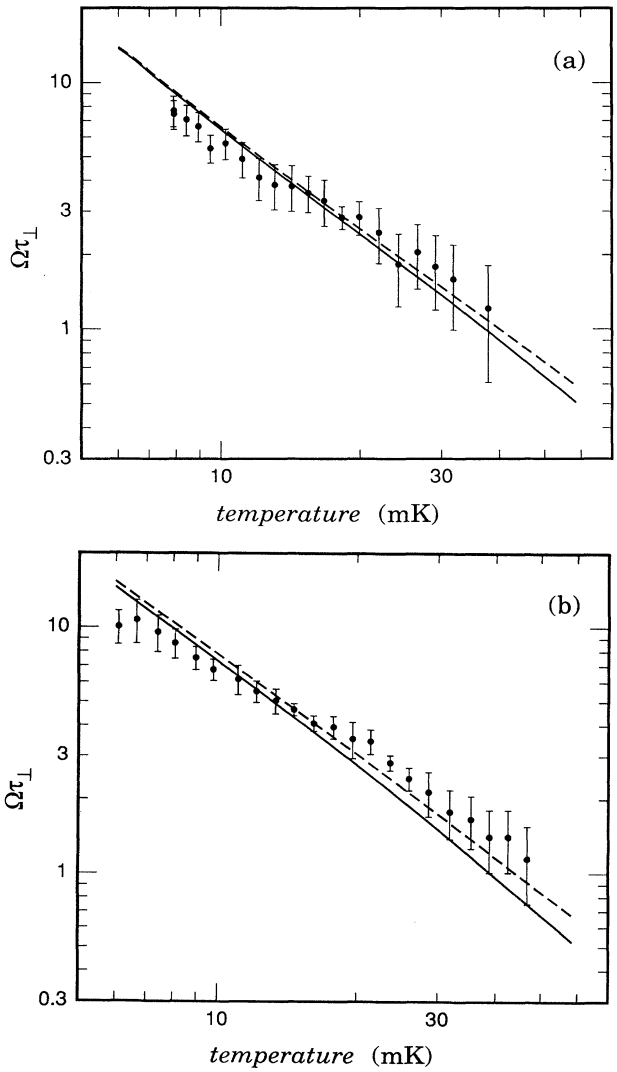

FIG. 7. Spin-rotation parameter $\Omega\tau_\perp$ for (a) $x_3=1.82\times10^{-3}$ and (b) $x_3=6.26\times10^{-4}$. The solid and dashed curves show theoretical calculations using the same $V(q)$ and s-wave approximation as for Fig. 6.

Calculations of $D_\perp/\Omega\tau_\perp$ and $\Omega\tau_\perp$ using the recent method of Jeon and Mullin valid for arbitrary temperature and polarization[6,7] are also shown on Figs. 6 and 7. These calculations take as input the effective quasiparticle interaction $V(q)$, which has been variously interpreted as the Fourier transform of an effective ^{3}He-^{3}He potential, or as the scattering amplitude for ^{3}He quasiparticles with unlike spin as a function of the magnitude of the momentum transferred.[16] The two pictures are equivalent within the Born approximation, but the scattering-amplitude picture is probably preferable because it has a definite physical interpretation even if the Born approximation (or, more generally, the idea of representing the interaction in terms of a potential) breaks down. Also, it becomes possible to identify the s-wave scattering length a with the low-momentum-transfer limit $V(0)=4\pi\hbar^2a/m$. This is important because much theoretical work has been expressed in terms of a, and the initial expectation was that mixtures as dilute as used in these experiments could be accurately described using only s-wave scattering.[2]

The description of dilute mixtures using $V(q)$ has been questioned because calculations to date have omitted several effects, such as x_3 dependence due to the filled Fermi sphere at low T/T_F, and velocity dependence or nonlocality of the scattering amplitude, which make it depend upon the incident quasiparticle momenta in addition to the momentum transferred.[2] We note that the Fermi velocity in the present experiments (7–10 m/s) is much less than the ^{4}He sound speed (240 m/s). As the ^{3}He-^{3}He interaction is largely mediated by exchange of virtual ^{4}He phonons, the relatively low ^{3}He velocity gives some hope that velocity dependence of the interaction is negligible for these low concentrations and temperatures.

Several, slightly different forms for $V(q)$ have been proposed over the years as different experimental data and theoretical methods have become available.[33–36] Common features have been $V(0)<0$, giving an attractive interaction at small momentum transfer, and a crossover at larger q to $V(q)>0$. Because both the Fermi and thermal velocities are so small, the present experiments only probe the low-q portion of $V(q)$. In particular, the calculations show that only the first two terms in a power-series expansion of $V(q)$ (q^0 and q^2) are significant for these experiments. Therefore, we have attempted to fit our data by simply multiplying by an overall scaling factor the $V(q)$ proposed by Ebner[34] on the basis of

transport measurements at much higher concentrations and temperatures. The results of this fit may be considered physically significant to the extent that (a) the four, independent temperature-dependent functions we have measured ($D_\perp/\Omega\tau_\perp$ and $\Omega\tau_\perp$, each for two values of x_3) are all fit using the same scaling factor, and (b) the scaling factor is reasonably close to one, reflecting possible mild finite-temperature and finite-concentration corrections for the data used to construct this $V(q)$.

The solid curves in Figs. 6 and 7 show the best overall fit to the data, which was obtained by multiplying the Ebner $V(q)$ by 1.07. This gives $V(0)=-1.50\times10^{-38}$ erg cm^3 and $a=-1.21$ Å. The fit is satisfactory, with the exception of $D_\perp/\Omega\tau_\perp$ for the lower concentration and temperatures below 20 mK. In this case only, the experimental data is systematically greater than the predictions of the Jeon and Mullin theory, by as much as 25%. Although the fit shown was obtained without adjusting the relative strength of the q^2 term in $V(q)$, calculations have been carried out showing no reasonable variation of this term can remove the discrepancy in $D_\perp/\Omega\tau_\perp$ at low temperature without degrading the fit of the rest of the data to the theory. The physical reason is that the effect of the q^2 term is greatest at higher concentrations and temperatures, where the fit is already good.

We may speculate that the discrepancy reflects some polarization dependence that has not been incorporated in the calculations, since the polarization is greatest for low T and low x_3. Alternatively, the discrepancy might be a sign of new physics at the interface between the dilute solution and the silica cell wall. For example, some calculations have suggested the possibility of a bound state for ^{3}He near the wall[37] (it is well known that the layer immediately adjacent to the wall is preferentially occupied by ^{4}He). A reactive boundary condition on M_+ that represented the storage of magnetization in such a layer (rather than its relaxation) would primarily affect $D_\perp/\Omega\tau_\perp$.

The dashed curves in Figs. 6 and 7 show calculations using the s-wave approximation; that is, setting $V(q)$ constant equal to $V(0)$ (using the same value as for the solid curves). The effect of making the s-wave approximation is negligible for $\Omega\tau_\perp$ but it significantly lowers $D_\perp/\Omega\tau_\perp$. The effect persists to arbitrarily low T because the typical momentum transfer in quasiparticle scattering is of the order of the Fermi momentum, even at $T=0$. While it would be possible to achieve reasonable agreement between the $D_\perp/\Omega\tau_\perp$ data and the s-wave calculation by decreasing $|a|$, this would destroy the agreement with $\Omega\tau_\perp$. Our conclusion is that much more dilute solutions at much lower temperatures would be required for the s-wave approximation to be accurate.

Finally, we compare the values of $V(0)$ and a deduced from these experiments with earlier results. Clearly the 7% increase over the Ebner value is reasonable in view of plausible accuracies for both sets of transport calculations, as well as the nonlocal or concentration-dependent effects expected for the earlier experiments at high T and x_3. In any case, this shift is of the same order as the differences between the various forms for $V(q)$ that have been proposed.

Attempts have been made to describe transport in ^{3}He-^{4}He mixtures purely in terms of s-wave scattering.[2] We may compare these results with the s-wave scattering length deduced from our experiments, $a=-1.21$ Å. A fit of a variety of transport data to the s-wave theory[2] gave $a=-1.5$ Å, and more recently a fit of the s-wave theory to $D_\perp/\Omega\tau_\perp$ data from Ref. 18 suggested[2] a much weaker $a=-0.6\pm0.1$ Å. However, our experimental values for $D_\perp/\Omega\tau_\perp$ do not agree with Ref. 18.

Both the Ebner $V(q)$ and most earlier determinations of a were derived from data at relatively large x_3. It is more significant to compare our result for the interaction strength, $V(0)=-1.50\times10^{-38}$ erg cm^3, with other experiments at very low T and x_3. These should all be accurately described by the same quadratic $V(q)$ (that is, the q^0 and q^2 terms should agree). Recently there have been experiments measuring several different transport properties in this regime, in addition to the work reported here. Owers-Bradley *et al.* measured the damping of second sound,[38] which is sensitive to thermal conductivity and viscosity, and deduced a significantly weaker $V(0)=-1.15\times10^{-38}$ erg cm^3. Nunes *et al.* measured the longitudinal spin-diffusion coefficient $D_\parallel$ using inversion recovery in a two-chamber experiment.[39] They found $D_\parallel$ was well fit by the Jeon and Mullin theory using the Ebner $V(q)$, for which $V(0)=-1.40\times10^{-38}$ erg cm^3. Most recently we have reported a direct measurement of the viscosity using a vibrating-wire viscometer.[40] We find that the $V(q)$ that best fits the spin-transport measurements reported here [1.07 times the Ebner $V(q)$] also gives excellent agreement with both the absolute value of the viscosity and its polarization dependence.

Taken together, the experimental results are largely consistent with the calculations of Jeon and Mullin[6,7] for a half-polarized, half-degenerate Fermi gas. The quasiparticle scattering amplitude at low momentum transfer appears to be precisely determined by the experimental results. Future work must strive to understand processes occurring at boundaries or surfaces,[41] as well as the nonlinear effects[39] that occur when the polarization is tipped far from equilibrium.

ACKNOWLEDGMENTS

The authors wish to thank Professor W. J. Mullin for providing extensive calculations of the transport theory of Refs. 6 and 7, as well as for many useful discussions. We also thank D. T. Sprague and Professor Kenneth Langley for suggesting the index-matching method for measuring the spin-wave cavity, and Dr. Gerard Vermeulen for work on several aspects of the experiments. This work was supported by NSF Grant Nos. DMR 8720746 and DMR 9100044.

[1]*Spin Polarized Quantum Systems,* edited by S. Stringari (World-Scientific, Singapore, 1989).
[2]A. E. Meyerovich, in *Helium Three,* edited by W. P. Halperin and L. P. Pitaevskii (North-Holland, Amsterdam, 1990), Chap. 13; A. E. Meyerovich, in *Progress in Low Temperature Physics,* edited by D. F. Brewer (North-Holland, Amsterdam, 1987), Vol. XI.
[3]E. P. Bashkin, Pis'ma Zh. Eksp. Teor. Fiz. **33**, 11 (1981) [JETP Lett. **33**, 8 (1981)].
[4]C. Lhuillier and F. Laloë, J. Phys. (Paris) **43**, 197 (1982); **43**, 225 (1982).
[5]L. P. Lévy and A. E. Ruckenstein, Phys. Rev. Lett. **52**, 1512 (1984).
[6]J. W. Jeon and W. J. Mullin, J. Phys. (Paris) **49**, 1691 (1988); Phys. Rev. Lett. **62**, 2691 (1989).
[7]J. W. Jeon and W. J. Mullin (unpublished).
[8]P. J. Nacher, G. Tastevin, M. Leduc, S. B. Crampton, and F. Laloë, J. Phys. (Paris) **45**, L441 (1984).
[9](a) B. R. Johnson, J. S. Denker, N. Bigelow, L. P. Lévy, J. H. Freed, and D. M. Lee, Phys. Rev. Lett. **52**, 1508 (1984); (b) N. P. Bigelow, J. H. Freed, and D. M. Lee, *ibid.* **63**, 1609 (1989).
[10]S. Schultz and G. Dunifer, Phys. Rev. Lett. **18**, 283 (1967).
[11]L. R. Corruccini, D. D. Osheroff, D. M. Lee, and R. C. Richardson, J. Low Temp. Phys. **8**, 229 (1972).
[12]D. Candela, N. Masuhara, D. S. Sherrill, and D. O. Edwards, J. Low Temp. Phys. **63**, 369 (1986).
[13]J. R. Owers-Bradley, H. Chocholacs, R. M. Mueller, Ch. Buchal, M. Kubota, and F. Pobell, Phys. Rev. Lett. **51**, 2120 (1983); R. M. Bowley and J. R. Owers-Bradley, J. Low Temp. Phys. **63**, 331 (1986).
[14]D. Einzel, G. Eksa, Y. Hirayoshi, T. Kopp, and P. Wölfle, Phys. Rev. Lett. **53**, 2312 (1984).
[15]H. Ishimoto, H. Fukuyama, T. Fukuda, T. Tazaki, and S. Ogawa, Phys. Rev. B **38**, 6422 (1988).
[16]G. Baym and C. Pethick, in *The Physics of Liquid and Solid Helium,* edited by K. H. Bennemann and J. B. Ketterson (Wiley, New York, 1978), Pt. II, p. 123.
[17]A. Ghozlan and E. Varoquaux, Ann. Phys. (Paris) **4**, 239 (1979); R. M. Bowley, J. Low Temp. Phys. **61**, 291 (1985). We have used this value of m/m_3 for our data analysis.
[18]W. J. Gully and W. J. Mullin, Phys. Rev. Lett. **52**, 1810 (1984).
[19]Some of this work has been briefly reported in D. Candela, D. R. McAllaster, L-J. Wei, and G. A. Vermeulen, Phys. Rev. Lett. **65**, 595 (1990).
[20]A. E. Meyerovich, Phys. Lett. **107A**, 177 (1985).
[21]A. J. Leggett, J. Phys. C **3**, 448 (1970).
[22]V. P. Silin, Zh. Eksp. Teor. Fiz. **33**, 1227 (1957) [Sov. Phys. JETP **6**, 945 (1958)].
[23]K. Miyake, W. J. Mullin, and P. C. E. Stamp, J. Phys. (Paris) **46**, 663 (1985).
[24]*Handbook of Mathematical Functions,* edited by M. Abramowitz and I. A. Stegun (Dover, New York, 1965), Sec. 10.1.
[25]D. Candela and D. R. McAllaster, Cryogenics **31**, 94 (1991).
[26]D. S. Greywall and P. A. Bush, J. Low Temp. Phys. **46**, 451 (1982).
[27]D. S. Greywall, Phys. Rev. B **33**, 7520 (1986).
[28]D. Candela and D. R. McAllaster, Rev. Sci. Instrum. **62**, 522 (1991).
[29]D. I. Hoult and R. E. Richards, J. Magn. Reson. **22**, 561 (1976).
[30]J. R. Owers-Bradley, R. M. Bowley, and P. C. Main, J. Low Temp. Phys. **60**, 243 (1985).
[31]J. R. Owers-Bradley, D. Wightman, R. M. Bowley, and A. Bedford, Physica B **165&166**, 729 (1990).
[32]K. S. Bedell and D. E. Meltzer, Phys. Rev. B **33**, 4543 (1986).
[33]J. Bardeen, G. Baym, and D. Pines, Phys. Rev. **156**, 207 (1967).
[34]C. Ebner, Phys. Rev. **156**, 222 (1967).
[35]J. Landau, J. T. Tough, N. R. Brubaker, and D. O. Edwards, Phys. Rev. A **2**, 2472 (1970).
[36]E. S. Murdock, K. R. Mountfield, and L. R. Corruccini, J. Low Temp. Phys. **31**, 581 (1978).
[37]J. Treiner (private communication).
[38]J. R. Owers-Bradley, P. C. Main, R. J. Church, T. M. M. Hampson, G. McHale, and R. M. Bowley, J. Low Temp. Phys. **77**, 327 (1989).
[39]G. Nunes, C. Jin, A. M. Putnam, and D. M. Lee, Phys. Rev. Lett. **65**, 2149 (1990).
[40]D. Candela, L-J. Wei, D. R. McAllaster, and W. J. Mullin, Phys. Rev. Lett. **67**, 330 (1991).
[41]A. E. Meyerovich, Physica B **165&166**, 747 (1990).